Journal of Environmental Chemical Engineering 5 (2017) 1866–1873

Contents lists available at ScienceDirect

Journal of Environmental Chemical Engineering

journal homepage: www.elsevier.com/locate/jece

Research paper

Highly efficient removal of Pb^{2+} by a polyoxomolybdate-based organic-inorganic hybrid material {$(4\text{-Hap})_4[Mo_8O_{26}]$}

Xue-Dong Du[a,b], Chong-Chen Wang[a,b,*], Jun Zhong[a], Jian-Guo Liu[a], Yu-Xuan Li[a], Peng Wang[a]

[a] Beijing Key Laboratory of Functional Materials for Building Structure and Environment Remediation, Beijing University of Civil Engineering and Architecture, Beijing 100044, China
[b] Key Laboratory of Urban Stormwater System and Water Environment (Ministry of Education), Beijing University of Civil Engineering and Architecture, Beijing 100044, China

ARTICLE INFO

Article history:
Received 27 December 2016
Received in revised form 6 March 2017
Accepted 24 March 2017
Available online 25 March 2017

Keywords:
Organic-inorganic hybrid compound
Adsorption
Pb^{2+}
Electrostatic interactions
Ion exchange

ABSTRACT

An organic-inorganic hybrid compound, $(4\text{-Hap})_4[Mo_8O_{26}]$ (4-ap = 4-aminopyridine) (**BUC-14**), was synthesized via hydrothermal method, and utilized to conduct adsorptive uptake of typical heavy metal ion (Pb^{2+}), in which some key parameters on Pb^{2+} adsorption and possible mechanism were investigated. The **BUC-14** results in excellent adsorption performance for Pb^{2+} from simulated wastewater, and the maximum uptake capacity is 1105.7 mg/g at 298 K. The kinetics behavior and equilibrium isotherm were well described using pseudo-second-order and Langmuir model, respectively. The adsorption process was thought to be divided two stages as electrostatic adsorption and ion exchange adsorption. Finally, the adsorption mechanism was proposed.

1. Introduction

Heavy metal pollution which can cause brain damage and disease to humans and other species had become a serious threat to environment [1]. If someone drinks water containing Pb^{2+} ions for a long term, even if in a very low concentration, it would lead to serious disorders like nausea, convulsions, coma, renal failure, cancer, even subtle effects on metabolism and intelligence [2]. Up to now, many techniques had been introduced to remove Pb^{2+} ion from waste water, such as ion exchange [3], co-precipitation [4], membrane filtration [5], adsorption [6], and so on [7–9]. Among them, the adsorption technique is the most extensively adopted one considering its low cost, ease operation and high efficiency, especially for organic dyes and heavy metal ions with low concentration [10]. As a result, continuous efforts are being made to prepare adsorbents with excellent performance [11,12].

Design and assembly of organic-inorganic hybrid materials based on the polyoxomolybdate anions are currently of great interest in the field of material chemistry and crystal engineering due to that they can provide versatile architectures and potential applications in electrochemistry [13], adsorption [14], fluorescence [15], photocatalysis [16] and magnetism [17]. A novel organic-inorganic hybrid material named $(4\text{-Hap})_4[Mo_8O_{26}]$ (**BUC-14**) was synthesized under hydrothermal conditions by Zhang et al. [18], which exhibited ultra-high uptake efficiency and capacity to methylene blue (MB). **BUC-14** preferred to uptake cationic MB from MB/MO (MO = methyl orange) mixture because of its negative zeta potential of −46.7 mV. **BUC-14** could adsorb both cationic MB and RhB (RhB = Rhodamine B), but it tended to adsorb MB from MB/RhB (RhB = Rhodamine B) mixture because of the well match between the molecular size of MB and its porosity size. Considering that **BUC-14** could uptake cationic species, and also being encouraged by the excellent performances of Hg^{2+} ions in similar organic – inorganic hybrid crystalline materials [1,19,20], within this paper, Pb^{2+} was selected as a heavy metal model to further verify the adsorption performance of **BUC-14**. The involved kinetic models, isotherm models and the thermodynamic parameters were analyzed and calculated. A continuous flow fixed bed column experiment was conducted to provide information for large-scale practical operation. And the possible adsorption

* Corresponding author at: Beijing Key Laboratory of Functional Materials for Building Structure and Environment Remediation, Beijing University of Civil Engineering and Architecture, Beijing, 100044, China.
E-mail address: chongchenwang@126.com (C.-C. Wang).

http://dx.doi.org/10.1016/j.jece.2017.03.028
2213-3437/

mechanism was proposed, which was affirmed by XPS, SEM-EDS and FTIR analyses.

2. Experimental

2.1. Materials

Cadmium chloride hydrate ($CdCl_2{\cdot}2.5H_2O$), ammonium molybdate tetrahydrate ($H_{24}Mo_7N_6O_{24}{\cdot}4H_2O$), 4-aminopyridine (4-ap) and lead standard solution (1000 mg/L) were purchased from J&K Scientific Ltd and used without further purification.

2.2. Synthesis of organic-inorganic hybrid compound [(4-Hap)$_4$(Mo_8O_{26})] (**BUC-14**)

BUC-14 was synthesized according to the reported procedure by Zhang et al. [18]. A mixture of $CdCl_2{\cdot}2.5H_2O$ (0.3 mmol, 0.0685 g), ammonium molybdate tetrahydrate ($H_{24}Mo_7N_6O_{24}{\cdot}4H_2O$, 0.6 mmol, 0.7415 g) and 4-ap (0.3 mmol, 0.0280 g) with molar ratio of 1:2:1 was sealed in a 25 mL Teflon-lined stainless steel Parr bomb containing deionized H_2O (20 mL), heated at 443 K for 72 h, and then cooled down to room temperature. White block-like crystals of **BUC-14** were isolated, washed with deionized water and ethanol three times sequentially, and finally dried at 60 °C.

2.3. Characterization

Powder X-ray diffraction (PXRD) patterns of the samples were obtained with a Dandonghaoyuan DX–2700B diffractometer in the range of $2\theta = 5°–40°$ with Cu Kα radiation. The Fourier transform infrared (FTIR) spectra were recorded from KBr pellets on Nicolet 6700 spectrometer in the range of 4000–400 cm^{-1}. The surface area of the sample was obtained from N_2 adsorption-desorption isotherms at 77 K using Brunauer-Emmett-Teller nitrogen-helium absorption method (BET, V-Sorb 2800P, Gold APP Instruments Co., Ltd). The morphology and the elemental mapping were observed using a FEI Quanta 250 FEG scanning electron microscope (SEM) equipped with Bruker XFlash 5010 Energy Dispersive Spectrometer (EDS). X-ray photoelectron spectra (XPS) measurement was performed with Thermo ESCALAB 250XI. The surface charge of the particles was assessed by zeta potential measurements using the Malvern zeta sizer Nano ZS and by applying the field strength of 20 V/cm.

A 6545 Q-TOF LC/MS (Agilent Technologies) was used to detect the organic compounds in the solution after adsorption. The analytes were separated by an Agilent ZORBAX SB-Aq (1.8 μm, 2.1 × 50 mm) on an Agilent 1290 UHPLC equipped with a DAD detector. Acidified water (0.05% formic acid, *v*/*v*) and acetonitrile were used as mobile phase A and B, respectively. Gradient was programmed as follow: 0 min, 0% B; 1 min, 0% B; 2 min, 95% B. The column temperature was maintained at 308 K. The 6545 Q-TOF LC/MS was equipped with a Jet Stream electrospray ionization source (ESI). Parameters for analysis were set in both positive and negative ion modes. The optimal values of the ion source parameters were: capillary, +2000 V; drying gas temperature, 473 K; drying gas flow, 8.0 L/min; nebulizer pressure, 35 psi; shealth gas temperature, 573 K and shealth gas flow, 11.0 L/min. The MS data were processed using Mass Hunter Qualitative Analysis software (Agilent Technologies), which provided a list of possible elemental formulas. Molecular Structure Correlator software (Agilent Technologies) was employed to analyze the MS/MS spectra and to match the possible structures.

The leaked concentration of Mo from **BUC-14** in the solution after adsorption was determined by ICP-OES (Thermo Scientific iCAP 7200) at the wavelength of 202.03 nm, with the detection limit being 0.004 mg/L.

2.4. Adsorption performance towards Pb^{2+}

The adsorption performance of the as-synthesized **BUC-14** samples was investigated by assessing the removal efficiency of Pb^{2+} from the simulated wastewater prepared by dissolving Pb$(NO_3)_2$ in deionized water with pH = 1.0–1.2. A desired amount of **BUC-14** sample (0.0040 g) with a particle size less than 147 μm was added to 200 mL simulated Pb^{2+} aqueous solution with concentrations ranging from 18.0 mg/L to 26.0 mg/L in a 250 mL conical flask. The mixture was shaken at a constant speed of 140 rpm in a constant temperature water bath oscillator under temperatures 298 K, 308 K, 318 K and 328 K, respectively. After shaking for 3 h, the **BUC-14** sample was separated by filtration through a membrane filter (0.45 μm). The residual concentration of Pb^{2+} was determined by flame atomic absorption spectrophotometry (PinAAcle 900T).

2.5. Column study and selective adsorption

Fixed bed study was conducted in the solid phase extraction (SPE) columns (Φ = 1.0 cm, 6.5 cm in length). The solution containing 10 mg/L Pb^{2+} was passed up-to-bottom via the column containing 1.5 g **BUC-14** sample with a particle size less than 147 μm (packing height = 8 mm) at a flow rate of 10 mL/min. The residual Pb^{2+} concentrations of the treated solutions were determined by flame atomic absorption spectrophotometry (PinAAcle 900T). The equipment of column study is depicted as Fig. 1(b).

A desired amount of **BUC-14** sample (0.0040 g) was added to 500 mL simulated wastewater with Pb^{2+} (10.0 mg/L)/Cu^{2+} (10.0 mg/L) and Pb^{2+} (10.0 mg/L)/Cd^{2+} (10.0 mg/L) in a 1000 mL conical flask, respectively. Flame atomic absorption spectrophotometry (PinAAcle 900T) was used to determine the residual Pb^{2+}, Cu^{2+} and Cd^{2+} in the solutions after adsorption, which can identify the selective adsorption performance of **BUC-14** towards different heavy metals.

3. Results and discussion

3.1. Adsorption performance

3.1.1. Equilibrium studies (isotherm models)

The analyses of the isotherm data are important and necessary to fit corresponding equations, which can accurately describe the obtained results, and can be utilized for the design purpose. To investigate the sorption isotherm, three isotherm models including Langmuir, Freundlich, and Dubinin–Radushevich isotherm equations (as listed in Eqs. S1–S3) were utilized to describe the equilibrium adsorption data. Considering that each model possesses both advantages and disadvantages, five error functions (the corresponding equations being listed in Table S1) along with correction coefficient R^2 were introduced to determine the best fit adsorption isotherm [21]. The adsorption data fitted by three different isotherm models was shown in Table 2 and Fig. S1. The applicability of the isotherm models to adsorption behavior was determined by both the correlation coefficient (R^2) and the error functions values [22]. As shown in Table 2, the R^2 values of the Langmuir isotherm were greater than those of the other two isotherms for the adsorption of Pb^{2+}, and the various error function values of Langmuir isotherm were smaller than those of the other two isotherms. This implied that the adsorption of Pb^{2+} onto **BUC-14** adsorbent was better described by the Langmuir model than Freundlich, and Dubinin–Radushevich ones. As listed in Table 1 and 2, the predictable maximum adsorption capacities of **BUC-14** for Pb^{2+} ranged from 1105.7 mg/g to 1166.8 mg/g with the temperature increasing from 298 K to 328 K. The q_m values of Pb^{2+}

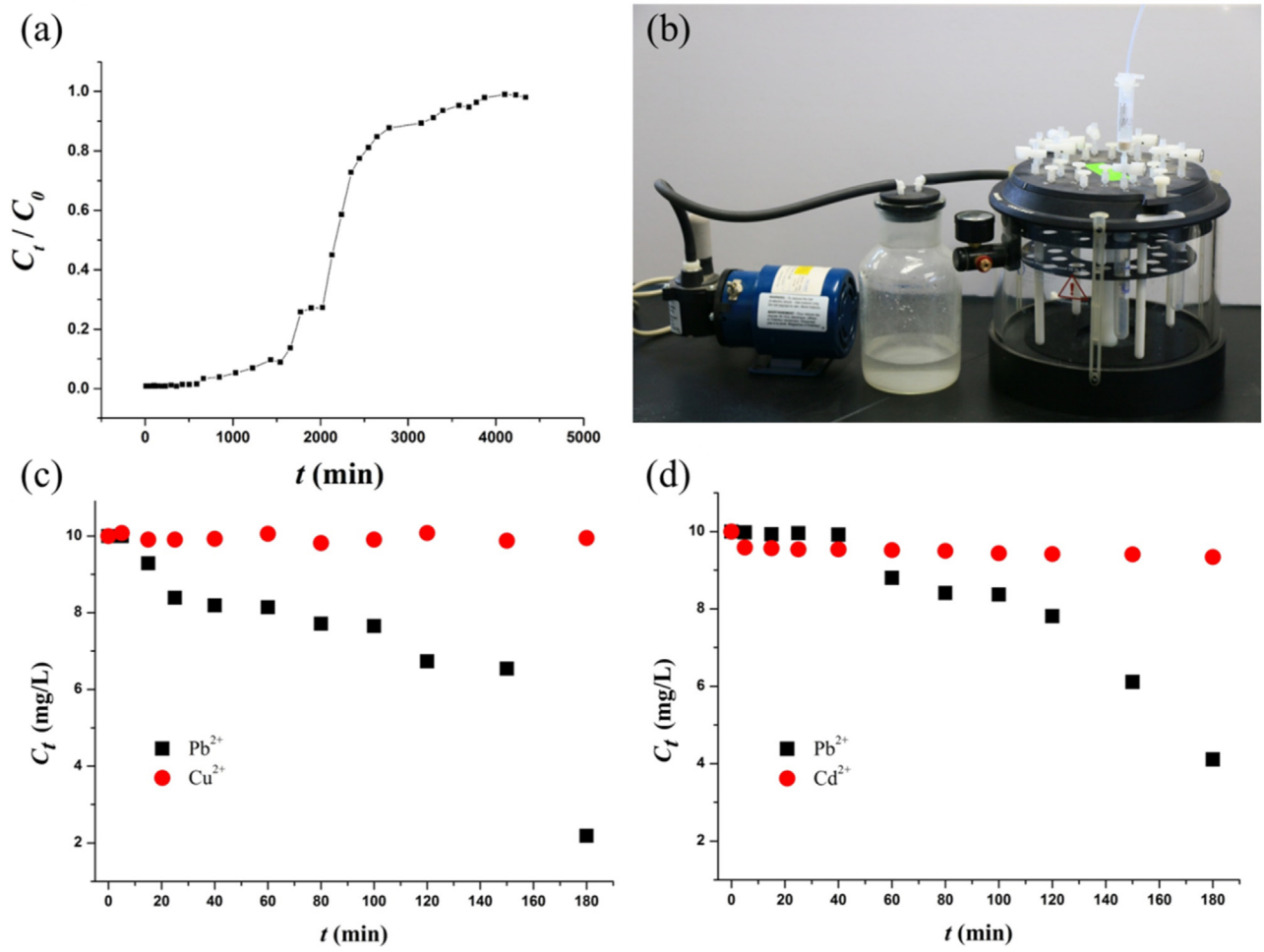

Fig. 1. (a) Breakthrough curves for **BUC-14** (C_t is the concentration of the Pb^{2+} in the effluent at time). (b) Equipment of column study. (c) Pb^{2+} and Cu^{2+} removal on **BUC-14** from their mixed solution at 25 °C and pH 2.65. (d) Pb^{2+} and Cd^{2+} removal on **BUC-14** from their mixed solution at 25 °C and pH 2.72.

BUC-14 adsorbent were compared with those of its counterparts as listed in Table 1, in which it can be found that the q_m value of **BUC-14** adsorbent was much higher than most of the adsorbents reported previously, including but not limited to amino-functionalized mesoporous silicas [23], *N*-methylimidazole modified palygorskite [24].

The essential characteristics and feasibility of the Langmuir isotherm were also determined in terms of a dimensionless constant separation factor (R_L), as calculated via Eq. S5 [25]. The R_L values can clarify the adsorption process to be irreversible ($R_L = 0$), favorable ($0 < R_L < 1$), linear ($R_L = 1$) or unfavorable ($R_L > 1$). The R_L values of Pb^{2+} adsorbed onto **BUC-14** ranged from 0.005 to 0.022 for the temperature from 298 K to 328 K, indicating that the adsorptions of Pb^{2+} onto **BUC-14** was favorable.

3.1.2. Thermodynamic parameters

In order to gain further insight into the Pb^{2+} adsorption process in the **BUC-14** adsorbent, the adsorption performances at various temperatures ranging from 298 K to 328 K were examined. It can be seen that the amount of adsorbed Pb^{2+} increased with the increasing temperature, implying that the adsorption of Pb^{2+} is endothermic reaction.

Table 1
Comparison of the adsorption capacities on various adsorbents.

Adsorbent	Adsorption capacity (mg/g)	Ref.
BUC-14	1105.7	This work
UiO_{66}-NH_2	1795.3	[26]
amino-functionalized mesoporous silicas	982.1	[23]
N-methylimidazole modified palygorskite	714.3	[24]
$CoFe_2O_4$-rGO	299.4	[27]
EDTA functionalized magnetic graphene oxide	268.4	[6]
Attapulgite clay@carbon	263.8	[28]
WO_3	248.9	[29]
Zinc silicate	210.0	[30]
Fe_3O_4-MnO_2	208.2	[31]
Ulmus tree leaves	201.1	[32]
Amino functionalized silica spheres	194.4	[33]
Hydroxyapatite	100.0	[34]

Table 2
Isotherm parameters and values of the error functions of the isotherm models.

Isotherm model	T/K	Parameters		R^2	ERRSQ	HYBRID	MPSD	ARE	EABS
Langmuir		K_L(L/mg)	q_m(mg/g)						
	298	1.67	1105.7	0.995	2436.8	2.77	0.003	0.102	91.2
	308	3.23	1126.0	0.999	1987.3	2.24	0.003	0.084	76.6
	318	5.97	1128.0	0.996	20530.6	21.52	0.023	0.248	237.5
	328	7.72	1166.8	0.991	63016.8	60.22	0.059	0.362	368.2
Freundlich		K_f(mg/g)	$1/n$						
	298	749.7	0.1751	0.845	4142.7	4.51	0.005	0.150	137.7
	308	872.8	0.1357	0.866	3811.7	4.11	0.004	0.139	132.0
	318	962.7	0.0820	0.605	11701.0	12.91	0.014	0.211	198.9
	328	1027.5	0.0589	0.121	54067.8	53.62	0.054	0.383	384.9
Dubunin-Radushkevich		K_{DR}	q_d(mg/g)						
	298	2.2×10^{-7}	1041.3	0.944	1116.8	1.21	0.001	0.079	73.0
	308	8.6×10^{-8}	1077.7	0.934	1337.2	1.46	0.002	0.071	65.4
	318	2.0×10^{-8}	1052.7	0.213	17953.9	19.57	0.021	0.240	226.6
	328	1.2×10^{-8}	1076.2	0.041	58338.4	58.48	0.060	0.416	418.6

In order to clarify the feasibility, favorability, spontaneity and even the mechanism of the ongoing adsorption process, thermodynamic parameters including standard Gibbs free energy (ΔG^o, kJ/mol), enthalpy change (ΔH^o, kJ/mol) and entropy change (ΔS^o, J/(mol K)), were calculated with the aid of data obtained from Langmuir adsorption isotherm via Eqs. S6 and S7 [35], as illustrated in Table 3. In general, free energy (ΔG^o) values between −20 and 0 kJ/mol suggests that physisorption process is dominated, while ΔG^o values ranging from −80 to −400 kJ/mol implies a chemisorption process [36]. In this study, the values of ΔG^o was found to decrease from −31.60 kJ/mol at 298 K to −38.95 kJ/mol at 328 K, indicating that the adsorption process of Pb^{2+} onto **BUC-14** adsorbent became more favorable at higher temperatures, which could also be confirmed from the corresponding maximum adsorption amount increase from 1105.7 mg/g at 298 K to 1166.8 mg/g at 328 K. The ΔG^o values from −31.60 kJ/mol to −38.95 kJ/mol also suggested that the sorption process was mainly controlled by physical sorption along with partial chemical sorption [36,37]. The positive value of ΔH^o (42.51 kJ/mol) indicated that the adsorption reaction is endothermic [38], which can be affirmed by the fact that the adsorption capacity increased with the increasing temperature. The positive ΔS^o value (249.24 J/(mol K)) for the sorption process implied the increase randomness at the solid-solution interface during the adsorption of Pb^{2+} onto **BUC-14** [39].

3.1.3. Kinetic studies

It was very important to predict the adsorption rate, adsorbate retention time and the reactor dimensions, which were all controlled by the system's kinetics [40]. Also, in order to design an effective adsorption process, it is highly necessary to have deep understanding and clear concept about the kinetics of the adsorption process. In this study, both the pseudo-first-order model [41] and the pseudo-second-order model [40] (the corresponding equations were depicted in ESI as Eqs. S8 and S9, respectively) were utilized to describe the adsorption kinetics process. The fittings of the pseudo-first-order and pseudo-second-order kinetic models to the kinetic experimental data for the Pb^{2+} adsorption onto **BUC-14** were illustrated in Fig. S2. The results listed in Table S2 and S3 demonstrated that the experimental q_e ($q_{e,exp}$) values (125.0 mg/g, 187.5 mg/g, 250.0 mg/g, 375.0 mg/g, and 401.3 mg/g) were in good accordance with the q_e ($q_{e,cal}$) values (128.2 mg/g, 192.3 mg/g, 256.4 mg/g, 400.0 mg/g, and 416.7 mg/g) calculated from the pseudo-second-order model, respectively. The corresponding correlation coefficient R^2 values were more close to unity of 1; and the Chi-square (χ^2) depicted as Eq. S10 listed in ESI of the pseudo-second-order model was much smaller than the pseudo-first-order model. All these results indicated that the pseudo-second-order model was suitably fitted to the kinetic data of Pb^{2+} adsorption onto **BUC-14**. The results also indicated that the increase of initial Pb^{2+} concentration led to increased equilibrium sorption capacity (q_e) and decreased rate constant of pseudo-second-order (k_2), while the lower initial concentration led to faster equilibrium and increased k_2 values (the rate constant of pseudo-second-order), which could be contributed to that there were plenty of available adsorption sites on the surface of **BUC-14** adsorbent in the initial stages [42].

Table 3
Thermodynamic parameters for sorption process of Pb^{2+} on **BUC-14** at different temperatures.

T/K	K_L (L/mol)	ΔG^o (kJ/mol)	ΔS^o (J/(mol K))	ΔH^o (kJ/mol)
298	345562	−31.60	249.24	42.51
308	669434	−34.35		
318	1236499	−37.09		
328	1598775	−38.95		

3.1.4. Analysis of column data and selective adsorption

To develop an industrial friendly method that can be utilized for the practical large-scale operation, a continuous flow fixed bed column is preferred due to that it is easy to operate and provides many useful parameters related to pollutants removal [43]. In the column operation, the adsorbents can be continuously in contact with a fresh solution, which implied that the concentration of the solution in contact with a given layer of the adsorbent in a column was relatively constant. The adsorption behavior and efficiency of the fixed bed column could be described in terms of the time for the appearance of breakthrough and the shape of the breakthrough curve, which was heavily influenced by bed height, flow rate and the feed solution concentration. Therefore, the column experiments can be used to predict how much effluent can be treated by the fixed bed and how long the fixed bed will last before regeneration.

The results of the fixed bed column studies in this study were illustrated in Fig. 1(a), which revealed that up to 360 min, there was few Pb^{2+} in the effluent ($C_t < 0.01$ mg/L). The adsorption capacity of the **BUC-14** packed bed was almost exhausted after 72 h of continuous inflow of Pb^{2+} solution. The adsorption capacity and the exhaustion time might be further increased via the increase of the adsorbent (**BUC-14**) loading mass [44].

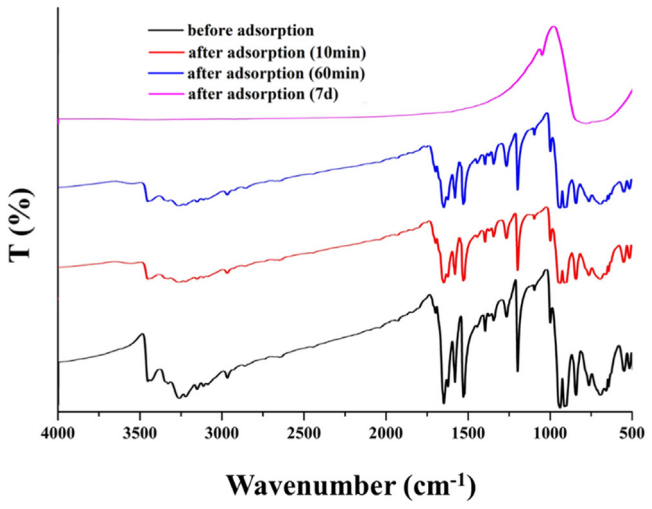

Fig. 2. FTIR spectra of BUC-14 before and after adsorption of Pb^{2+} from the solution at the first stage and the FTIR spectrum of $PbMoO_4$ formed in the second stage.

The total adsorbed Pb^{2+} (m_a) in the fixed bed for the initial influent concentration of 10 mg/L and the flow rate could be calculated using Eq. (1).

$$m_a = \frac{Q \cdot A}{1000} = \frac{Q}{1000} \int_{t=0}^{t=t_{tot}} C_{ad} \cdot dt \quad (1)$$

Where, Q refers to the volumetric flow rate in mL/min; t_{tot} is the total flow time (min). A is the area under the breakthrough curve that can be calculated by integrating the adsorbed concentration (C_{ad}) versus t plot using the Origin 9.1 software. m_{tot} is the total amount of Pb^{2+} influent through the fixed bed which can be calculated using Eq. (2).

$$m_{tot} = \frac{C_0 \cdot Q \cdot t_{tot}}{1000} \quad (2)$$

The total removal efficiency was calculated from the ratio of the total adsorbed Pb^{2+} amount *vs* the total amount of the added Pb^{2+} (m_{tot}) in the influent passed through the fixed bed using Eq. (3). The removal efficiency was as high as 96.81% in the first 360 min. The total adsorbed Pb^{2+}, m_{tot} and the total removal efficiency were 218.09 mg, 432.00 mg, and 50.48%, respectively. There was an instantaneous jump in effluent concentration from zero to the feed concentration when the breakthrough point (about 2000 min) was reached [44].

$$\text{total removal efficiency } (\%) = \frac{m_a}{m_{tot}} \times 100\% \quad (3)$$

In order to test the preferential adsorption of specified heavy metal species from their mixture, the selective adsorption experiments were designed. The results as shown in Fig. 1(c) and (d) revealed that Pb^{2+} ions were preferentially adsorbed by **BUC-14** from Pb^{2+}/Cu^{2+} and Pb^{2+}/Cu^{2+} mixtures, respectively, which implied that **BUC-14** can be used to efficiently separate and concentrate Pb^{2+} from the mixed solution of heavy metal ions.

For large-scale application, the leaking of Molybdenum (Mo) from **BUC-14** during the adsorption procedure was also a big issue. Therefore, the Mo contents determined with ICP-OES ranged from 0.09 mg/L to 0.113 mg/L, which was slightly higher than the limit values of 0.08 mg/L in drinking water set by EPA (EPA 822-R-04-005).

3.2. Proposed adsorption mechanism

According to the previously reported results of zeta potential by Zhang et al. [18], **BUC-13 h**ad an overall negative surface charge from pH = 2 to pH = 10. The zeta potential of **BUC-14** decreased with the increase of pH due to the protonation of N—H···O groups on its surface, which further indicated that there were plenty of positive sites on the surface. Electrostatic interactions between negative charges originated from $[Mo_8O_{26}]^{4-}$ and the positive charges of adsorbate (Pb^{2+} in this study) were responsible for the strong affinity between the **BUC-14** and Pb^{2+}. Previous studies had illuminated that the surface area was an important factor to influence the adsorption capacity [45,46]. But, in this study, **BUC-14** possessed inferior surface area (5.17 m^2/g) determined by N_2 sorption/desorption measurement [18], which implied that the strong affinity in binding with Pb^{2+} might not be assigned to its surface area. To further investigate the adsorption mechanism of Pb^{2+} onto **BUC-14**, FTIR, elemental mapping obtained from SEM, XRD, and XPS were used to analyze the composition, morphology and microstructure of **BUC-14** before and after uptake of Pb^{2+}.

The uptake of Pb^{2+} via **BUC-14** as absorbent was proposed to be attributed to both electrostatic interactions along with coordination interactions (the first stage process) and ion exchange (the second stage process). In the first stage (less than 60 min), Pb^{2+} ions were captured by **BUC-14** via electrostatic interactions between cationic Pb^{2+} and anionic surface charge of **BUC-14**, and even coordination interactions between Pb^{2+} and $—NH_2$ attached on pyridyl ring of 4-aminopyridine. Both the FTIR (Fig. 2) spectra and powder XRD

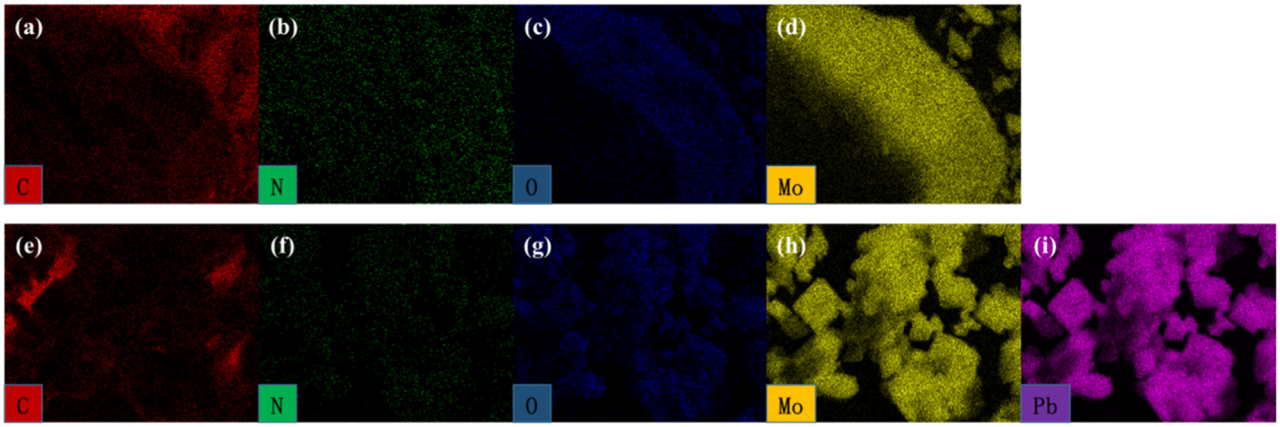

Fig. 3. (a)–(d) C, N, O and Mo elemental mapping of **BUC-14** (adsorption @10 min), (e)–(i) C, N, O, Mo and Pb elemental mapping of **BUC-14** after adsorption.

patterns (Figs. S3 and 4(a)) of **BUC-14** before adsorption and after adsorption were almost consistent with the corresponding ones of as prepared **BUC-14**, indicating a good stability of the crystalline sample. The elemental mapping obtained from SEM showed that the presence of Pb in **BUC-14** after adsorbing Pb^{2+} besides C, N, O, and Mo in the as-prepared **BUC-14** (as shown in Fig. 3). Furthermore, the uptake of Pb^{2+} onto **BUC-14** can be confirmed by XPS, in which the XPS spectra signals of Pb^{2+} with binding energy of 138.3 eV (Pb 4f) could be observed, as shown in Fig. 4(c). In the first stage, the functional groups of **BUC-14** like —NH_2 and Mo—O were proposed

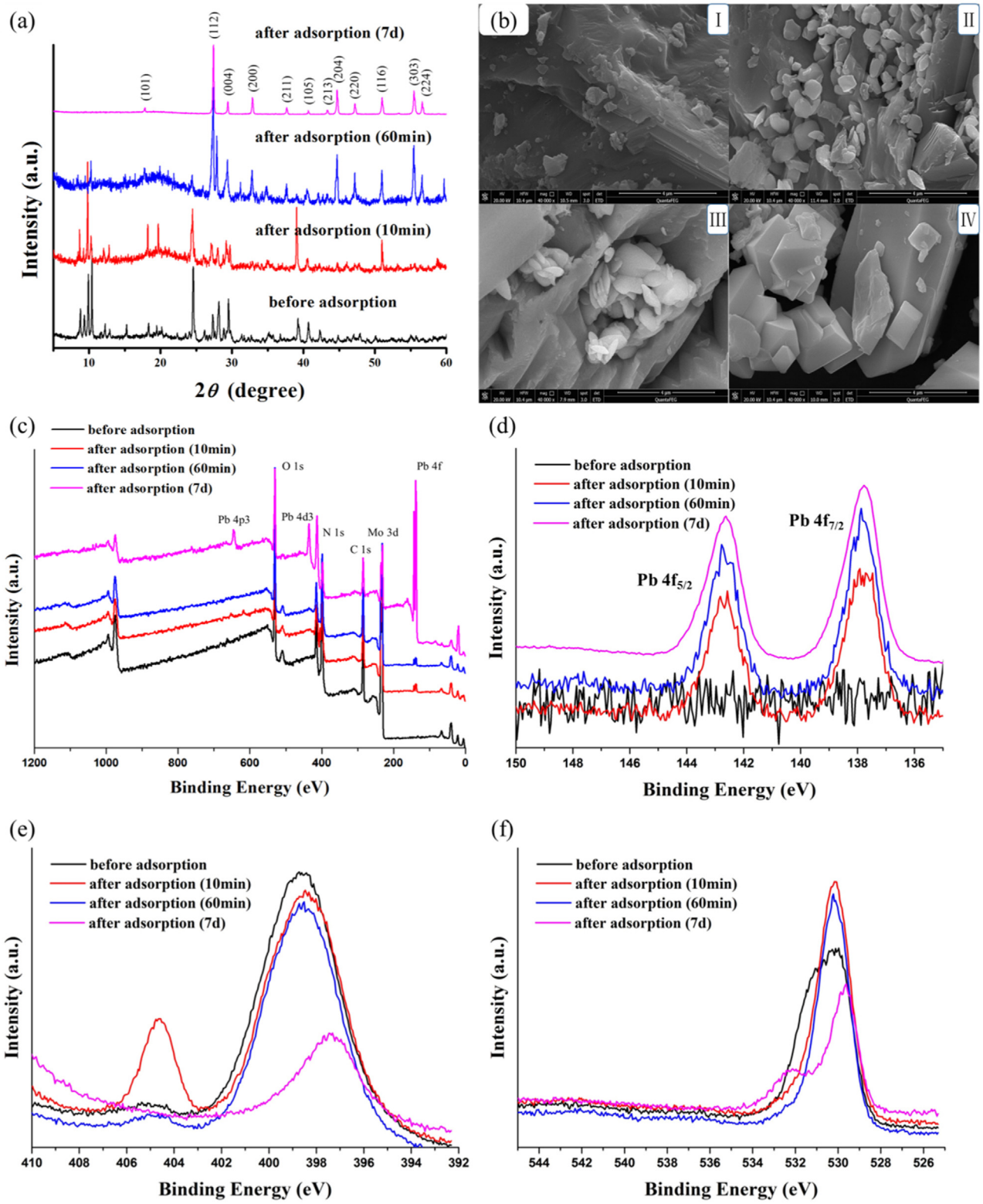

Fig. 4. (a) Comparison of XRD patterns of **BUC-14** before and after adsorption of Pb^{2+}. (b) SEM of **BUC-14** before and after adsorption ((I) before adsorption, (II) after 10 min adsorption, (III) after 60 min adsorption, (IV) after 7 d adsorption). (c) Full range XPS spectra of **BUC-14** before and after adsorption of Pb^{2+}, (d) XPS spectra of Pb 4f, (e) XPS spectra of N1s. (f) XPS spectra of O1s.

to play a key role in the removal of Pb^{2+}. The bands at 3454 and 3266 cm^{-1} (Fig. 2) in the FTIR spectra are assigned to the symmetric and asymmetric vibrations of $—NH_2$, the intense of above mentioned bands decreased due to the coordination of N in amidogen ($—NH_2$) with Pb^{2+} [26,47], which was confirmed by the presence of new peak at 404.8 eV in XPS spectra of **BUC-14** absorbing Pb^{2+}, as depicted in Fig. 4(e).

In the second stage, the uptake of Pb^{2+} could be assigned to the ion exchange between protonated 4-aminopyridine and Pb^{2+}, which was affirmed by the detection of free 4-aminopyridine in the solution from the information provided via Q-TOF-MS equipped with ESI, as shown in Figs. S4–S5. The XPS spectra as shown in Fig. 4(d) of the final product in the second stage revealed that the peaks at 142.7 eV (Pb $4f_{5/2}$) and 137.8 eV (Pb $4f_{7/2}$) were ascribed to PbO which was originated from Pb^{2+} ion of the $PbMoO_4$ [48,49], suggesting the formation of a new lead compound. The peaks in the curve for O1 s in final product obtained after adsorption at the 7th day were attributed to the bond of Mo—O at 529.3 eV and the bond of Pb—O at 532.1 eV as shown in Fig. 4(f) [49]. The peaks of PXRD pattern of the final product as depicted in Fig. 4(a) perfectly matched with the ones of $PbMoO_4$ (JCPDS card no. 164725), implying the formation of $PbMoO_4$ resulted from the complete ion exchange between protonated 4-aminopyridine and Pb^{2+} (as illustrated in Eq. (4)), just similar to the formation of $PbWO_4$ previously reported by Liu et al. [29]. The SEM images (Fig. 4(b)) also illustrated the change of **BUC-14**. The calculated value obtained with the aid of Eq. (4) indicated that 1.0 g of **BUC-14** could reaction with 1029.1 mg Pb^{2+}, which accorded well with the calculated maximum adsorption capacity (1105.7 mg/g) through Langmuir model. The formation of $PbMoO_4$ can also be affirmed by its FTIR spectra, which matched nicely with the FTIR spectra of $PbMoO_4$ in previous reported papers [50,51]. It was interesting to note that the final reaction product of $PbMoO_4$ was a potential photocatalyst [52,53], implying the sustainable and recyclable usage of the **BUC-14**.

$$C_{20}H_{28}N_8Mo_8O_{26} + 8Pb^{2+} + 6H_2O = 4C_5H_6N_2 + 8PbMoO_4 + 16H^+ \quad (4)$$

4. Conclusion

In all, $[(4\text{-Hap})_4(Mo_8O_{26})]$ (**BUC-14**) exhibited excellent performance to remove Pb^{2+} from simulated wastewater, and the adsorption process was proposed to be divided into two stages. In the first stage, the adsorption process followed pseudo-second-order kinetic model as well as Langmuir isotherms. The adsorption of Pb^{2+} onto **BUC-14** at various temperatures showed that the corresponding adsorption process was spontaneous (negative ΔG_0), endothermic (positive ΔH_0) and the randomness increases (positive ΔS_0). It was supposed that Pb^{2+} was adsorbed both through electrostatic attractions and coordination interactions in the first stage. In the second stage, the mechanism was proposed that ion exchange between protonated 4-aminopyridine and Pb^{2+}, which were proved by various characterization techniques like SEM-EDS, XRD, XPS and even Q-TOF-MS. The column study indicated **BUC-14** possessed a wide and potential application in practical engineering. **BUC-14** exhibited excellent selective adsorption of Pb^{2+} from the heavy metals matrix. Further researches should be carried out to clarify the adsorptive activities on other heavy metal ions and the photocatalytic performance of the finally obtained $PbMoO_4$.

Acknowledgments

This work was supported by the National Natural Science Foundation of China (51578034), the Beijing Natural Science Foundation & Scientific Research Key Program of Beijing Municipal Commission of Education (KZ201410016018) and Beijing Talent Project (2016023).

Appendix A. Supplementary data

Supplementary data associated with this article can be found, in the online version, at http://dx.doi.org/10.1016/j.jece.2017.03.028.

References

[1] B. Li, Y. Zhang, D. Ma, Z. Shi, S. Ma, Mercury nano-trap for effective and efficient removal of mercury(II) from aqueous solution, Nat. Commun. 5 (2014) 5537–5537.
[2] Y.-H. Li, Z. Di, J. Ding, D. Wu, Z. Luan, Y. Zhu, Adsorption thermodynamic, kinetic and desorption studies of Pb^{2+} on carbon nanotubes, Water Res. 39 (2005) 605–609.
[3] A. Smara, R. Delimi, E. Chainet, J. Sandeaux, Removal of heavy metals from diluted mixtures by a hybrid ion-exchange/electrodialysis process, Sep. Purif. Technol. 57 (2007) 103–110.
[4] W. Wang, Y. Hua, S. Li, W. Yan, W.-X. Zhang, Removal of Pb(II) and Zn(II) using lime and nanoscale zero-valent iron (nZVI): a comparative study, Chem. Eng. J. 304 (2016) 79–88.
[5] C. Blöcher, J. Dorda, V. Mavrov, H. Chmiel, N. Lazaridis, K. Matis, Hybrid flotation-membrane filtration process for the removal of heavy metal ions from wastewater, Water Res. 37 (2003) 4018–4026.
[6] L. Cui, Y. Wang, L. Gao, L. Hu, L. Yan, Q. Wei, B. Du, EDTA functionalized magnetic graphene oxide for removal of Pb(II), Hg(II) and Cu(II) in water treatment: adsorption mechanism and separation property, Chem. Eng. J. 281 (2015) 1–10.
[7] M. Ghaedi, A. Shokrollahi, K. Niknam, E. Niknam, A. Najibi, M. Soylak, Cloud point extraction and flame atomic absorption spectrometric determination of cadmium(II) lead(II), palladium(II) and silver(I) in environmental samples, J. Hazard. Mater. 168 (2009) 1022–1027.
[8] A. Karbassi, S. Nadjafpour, Flocculation of dissolved Pb, Cu Zn and Mn during estuarine mixing of river water with the Caspian Sea, Environ. Pollut. 93 (1996) 257–260.
[9] J. Cadotte, R. Petersen, R. Larson, E. Erickson, A new thin-film composite seawater reverse osmosis membrane, Desalination 32 (1980) 25–31.
[10] X.-Y. Yu, T. Luo, Y.-X. Zhang, Y. Jia, B.-J. Zhu, X.-C. Fu, J.-H. Liu, X.-J. Huang, Adsorption of lead(II) on O_2-plasma-oxidized multiwalled carbon nanotubes: thermodynamics, kinetics, and desorption, ACS Appl. Mater. Interfaces 3 (2011) 2585–2593.
[11] C.-Y. Cao, J. Qu, F. Wei, H. Liu, W.-G. Song, Superb adsorption capacity and mechanism of flowerlike magnesium oxide nanostructures for lead and cadmium ions, ACS Appl. Mater. Interfaces 4 (2012) 4283–4287.
[12] C.-Y. Cao, J. Qu, W.-S. Yan, J.-F. Zhu, Z.-Y. Wu, W.-G. Song, Low-cost synthesis of flowerlike α-Fe_2O_3 nanostructures for heavy metal ion removal: adsorption property and mechanism, Langmuir 28 (2012) 4573–4579.
[13] H.-Y. Liu, H. Wu, J. Yang, Y.-Y. Liu, B. Liu, Y.-Y. Liu, J.-F. Ma, pH-Dependent assembly of 1D to 3D octamolybdate hybrid materials based on a new flexible bis-[(pyridyl)-benzimidazole] ligand, Cryst. Growth Des. 11 (2011) 2920–2927.
[14] H. Fu, C. Qin, Y. Lu, Z.M. Zhang, Y.G. Li, Z.M. Su, W.L. Li, E.B. Wang, An ionothermal synthetic approach to porous polyoxometalate-based metal-organic frameworks, Angew. Chem. Int. Ed. 51 (2012) 7985–7989.
[15] H. Wu, J. Yang, Y.-Y. Liu, J.-F. Ma, pH-Controlled assembly of two unusual entangled motifs based on a tridentate ligand and octamolybdate clusters: 1D + 1D→ 3D poly-pseudorotaxane and 2D→ 2D→ 3D polycatenation, Cryst. Growth Des. 12 (2012) 2272–2276.
[16] H.-Y. Liu, L. Bo, J. Yang, Y.-Y. Liu, J.-F. Ma, H. Wu, Two novel inorganic-organic hybrid materials constructed from two kinds of octamolybdate clusters and flexible tetradentate ligands, Dalton Trans. 40 (2011) 9782–9788.
[17] X.-Y. Wu, P. Dong, R. Yu, Q.-K. Zhang, X. Kuang, S.-C. Chen, Q.-P. Lin, C.-Z. Lu, A 2D polyoxometalate-based complex: spin-canting and metamagnetism, CrystEngComm 13 (2011) 3686–3688.
[18] Y.Q. Zhang, C.C. Wang, T. Zhu, P. Wang, S.J. Gao, Ultra-high uptake and selective adsorption of organic dyes with a novel polyoxomolybdate-based organic-inorganic hybrid compound, RSC Adv. 5 (2015) 45688–45692.
[19] C. Abney, J. Gilhula, K. Lu, W. Lin, Metal-organic framework templated inorganic sorbents for rapid and efficient extraction of heavy metals, Adv. Mater. 26 (2014) 7993–7997.
[20] K.-K. Yee, N. Reimer, J. Liu, S.-Y. Cheng, S.-M. Yiu, J. Weber, N. Stock, Z. Xu, Effective mercury sorption by thiol-laced metal-organic frameworks: in strong acid and the vapor phase, J. Am. Chem. Soc. 135 (2013) 7795–7798.
[21] Y. Ho, J. Porter, G. McKay, Equilibrium isotherm studies for the sorption of divalent metal ions onto peat: copper, nickel and lead single component systems, Water Air Soil Pollut. 141 (2002) 1–33.
[22] M. Hadi, M.R. Samarghandi, G. Mckay, Equilibrium two-parameter isotherms of acid dyes sorption by activated carbons: study of residual errors, Chem. Eng. J. 160 (2010) 408–416.
[23] S. Hao, Y. Zhong, F. Pepe, W. Zhu, Adsorption of Pb^{2+} and Cu^{2+} on anionic surfactant-templated amino-functionalized mesoporous silicas, Chem. Eng. J. 189 (2012) 160–167.

[24] Y. Chang, H. Liu, F. Zha, H. Chen, X. Ren, Z. Lei, Adsorption of Pb(II) by *N*-methylimidazole modified palygorskite, Chem. Eng. J. 167 (2011) 183–189.
[25] I. Langmuir, The constitution and fundamental properties of solids and liguids, J. Am. Chem. Soc. 38 (1916) 2221–2295.
[26] N. Yin, K. Wang, L. Wang, Z. Li, Amino-functionalized MOFs combining ceramic membrane ultrafiltration for Pb(II) removal, Chem. Eng. J. 306 (2016) 619–628.
[27] Y. Zhang, L. Yan, W. Xu, X. Guo, L. Cui, L. Gao, Q. Wei, B. Du, Adsorption of Pb(II) and Hg(II) from aqueous solution using magnetic $CoFe_2O_4$-reduced graphene oxide, J. Mol. Liq. 191 (2014) 177–182.
[28] L.-F. Chen, H.-W. Liang, Y. Lu, C.-H. Cui, S.-H. Yu, Synthesis of an attapulgite clay@ carbon nanocomposite adsorbent by a hydrothermal carbonization process and their application in the removal of toxic metal ions from water, Langmuir 27 (2011) 8998–9004.
[29] B. Liu, J. Wang, J. Wu, H. Li, Z. Li, M. Zhou, T. Zuo, Controlled fabrication of hierarchical WO3 hydrates with excellent adsorption performance, J. Mater. Chem. A 2 (2014) 1947–1954.
[30] J. Qu, C.-Y. Cao, Y.-L. Hong, C.-Q. Chen, P.-P. Zhu, W.-G. Song, Z.-Y. Wu, New hierarchical zinc silicate nanostructures and their application in lead ion adsorption, J. Mater. Chem. 22 (2012) 3562–3567.
[31] J. Zhao, J. Liu, N. Li, W. Wang, J. Nan, Z. Zhao, F. Cui, Highly efficient removal of bivalent heavy metals from aqueous systems by magnetic porous Fe_3O_4-MnO_2: adsorption behavior and process study, Chem. Eng. J. 304 (2016) 737–746.
[32] M.R. Sangi, A. Shahmoradi, J. Zolgharnein, G.H. Azimi, M. Ghorbandoost, Removal and recovery of heavy metals from aqueous solution using Ulmus carpinifolia and Fraxinus excelsior tree leaves, J. Hazard. Mater. 155 (2008) 513–522.
[33] A.M. El-Toni, M.A. Habila, M.A. Ibrahim, J.P. Labis, Z.A.A.L. Othman, Simple and facile synthesis of amino functionalized hollow core-mesoporous shell silica spheres using anionic surfactant for Pb(II) Cd(II), and Zn(II) adsorption and recovery, Chem. Eng. J. 251 (2014) 441–451.
[34] S.-D. Jiang, Q.-Z. Yao, G.-T. Zhou, S.-Q. Fu, Fabrication of hydroxyapatite hierarchical hollow microspheres and potential application in water treatment, J. Phys. Chem. C 116 (2012) 4484–4492.
[35] Y. Bulut, Z. Tez, Adsorption studies on ground shells of hazelnut and almond, J. Hazard. Mater. 149 (2007) 35–41.
[36] A. Zaki, M. El-Sheikh, J. Evans, S. El-Safty, Kinetics and mechanism of the sorption of some aromatic amines onto amberlite IRA-904 anion-exchange resin, J. Colloid Interface Sci. 221 (2000) 58–63.
[37] V.K. Gupta, A. Mittal, D. Jhare, J. Mittal, Batch and bulk removal of hazardous colouring agent Rose Bengal by adsorption techniques using bottom ash as adsorbent, RSC Adv. 2 (2012) 8381–8389.
[38] J. Mittal, V. Thakur, A. Mittal, Batch removal of hazardous azo dye Bismark Brown R using waste material hen feather, Ecol. Eng. 60 (2013) 249–253.
[39] Y.-S. Ho, A.E. Ofomaja, Kinetics and thermodynamics of lead ion sorption on palm kernel fibre from aqueous solution, Process Biochem. 40 (2005) 3455–3461.
[40] Y.-S. Ho, Review of second-order models for adsorption systems, J. Hazard. Mater. 136 (2006) 681–689.
[41] Y.-S. Ho, Citation review of Lagergren kinetic rate equation on adsorption reactions, Scientometrics 59 (2004) 171–177.
[42] S. Zhou, Y. Shao, N. Gao, J. Deng, C. Tan, Equilibrium, kinetic, and thermodynamic studies on the adsorption of triclosan onto multi-walled carbon nanotubes, Clean Soil Air Water 41 (2013) 539–547.
[43] A.S. Michaels, Simplified method of interpreting kinetic data in fixed-bed ion exchange, Ind. Eng. Chem. Res. 44 (1952) 1922–1930.
[44] Z. Aksu, F. Gönen, Biosorption of phenol by immobilized activated sludge in a continuous packed bed: prediction of breakthrough curves, Process Biochem. 39 (2004) 599–613.
[45] D.-P. Li, Y.-R. Zhang, X.-X. Zhao, B.-X. Zhao, Magnetic nanoparticles coated by aminoguanidine for selective adsorption of acid dyes from aqueous solution, Chem. Eng. J. 232 (2013) 425–433.
[46] Y. Dong, B. Lu, S. Zang, J. Zhao, X. Wang, Q. Cai, Removal of methylene blue from coloured effluents by adsorption onto SBA-15, J. Chem. Technol. Biotechnol. 86 (2011) 616–619.
[47] L. Shen, W. Wu, R. Liang, R. Lin, L. Wu, Highly dispersed palladium nanoparticles anchored on UiO-66 (NH_2) metal-organic framework as a reusable and dual functional visible-light-driven photocatalyst, Nanoscale 5 (2013) 9374–9382.
[48] G. Gyawali, R. Adhikari, B. Joshi, T.H. Kim, V. Rodríguez-González, S.W. Lee, Sonochemical synthesis of solar-light-driven Ag-$PbMoO_4$ photocatalyst, J. Hazard. Mater. 263 (2013) 45–51.
[49] K. Dai, Y. Yao, H. Liu, I. Mohamed, H. Chen, Q. Huang, Enhancing the photocatalytic activity of lead molybdate by modifying with fullerene, J. Mol. Catal. A: Chem. 374 (2013) 111–117.
[50] A. Phuruangrat, B. Kuntalue, S. Artkla, S. Promnopas, W. Promnopas, S. Thongtem, T. Thongtem, Effect of lead salts on phase, morphologies and photoluminescence of nanocrystalline $PbMoO_4$ and $PbWO_4$ synthesized by microwave radiation, Mater. Sci. Pol. 34 (2016) 529–533.
[51] T.H. Kim, S.W. Lee, G. Gyawali, Y.H. Jo, T. Sekino, Synthesis of TiO_2-xNy/Ag-$PbMoO_4$ composite and their photocatalytic activity under simulated solar light irradiation, Int. J. Appl. Ceram. Technol. 12 (2015) 577–584.
[52] J. Bi, L. Wu, Y. Zhang, Z. Li, J. Li, X. Fu, Solvothermal preparation, electronic structure and photocatalytic properties of $PbMoO_4$ and $SrMoO_4$, Appl. Catal. B: Environ. 91 (2009) 135–143.
[53] M. Shen, Q. Zhang, H. Chen, T. Peng, Hydrothermal fabrication of $PbMoO_4$ microcrystals with exposed (001) facets and its enhanced photocatalytic properties, CrystEngComm 13 (2011) 2785–2791.